Vibrational Spectra and Structures of Ti−N2O and OTi−N−2: A Combined IR Matrix Isolation and Theoretical Study

ARTICLE *in* THE JOURNAL OF PHYSICAL CHEMISTRY A · JANUARY 2013

Impact Factor: 2.69 · DOI: 10.1021/jp309601e · Source: PubMed

THE JOURNAL OF PHYSICAL CHEMISTRY A

Article

pubs.acs.org/JPCA

Vibrational Spectra and Structures of Ti−N_2O and OTi−N_2: A Combined IR Matrix Isolation and Theoretical Study

Asma Marzouk, M. Esmaïl Alikhani,* Bruno Madebène, Benoît Tremblay,* and Jean-Pierre Perchard

UMR 7075, Laboratoire de Dynamique, Interactions et Réactivité (LADIR), UPMC Universite Paris 06, F-75005 Paris, France, and UMR 7075, Laboratoire de Dynamique, Interactions et Réactivité (LADIR), CNRS, F-75005 Paris, France

Supporting Information

ABSTRACT: The reaction of atomic titanium with nitrous oxide has been reinvestigated using matrix isolation in solid neon coupled to infrared spectroscopy and by quantum chemical methods. Our technique of sublimation of Ti atoms from a filament heated at about 1500 °C allowed the formation of three species: one Ti−N_2O pair of van der Waals (vdW) type characterized by small red shift with respect to N_2O monomer, and two isomers of OTi−N_2 pair where N_2 is in interaction with the OTi moiety either with end-on or side-on structure. Interconversion between these structures has been performed with several wavelengths. In the visible and near-ultraviolet the conversion vdW → OTi-N_2 (end-on) is observed with characteristic times strongly varying according to the wavelength. In the near-infrared the conversion OTi−N_2 (end-on) → OTi−N_2 (side-on) occurs, the vdW species remaining unchanged. These selectivities allow 8, 6, and 4 vibrational transitions to be assigned for vdW, ^{3}[OTi(η^1-NN)] (end-on), and ^{1}[OTi(η^2-NN)] (side-on), respectively. Electronic and geometrical structures are also investigated with double-hybrid functionals. It has been shown that the side-on geometry corresponds to the ground state of ^{1}[OTi(η^2-NN)] in the singlet electronic state. The theoretical vibrational analysis supports well the experimental attributions.

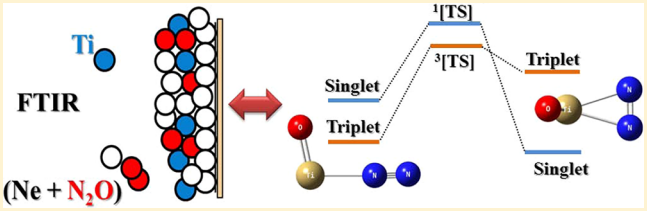

INTRODUCTION

In the course of a study devoted to the reactivity of the diatomic Ti_2 with respect to nitrous oxide N_2O in neon matrix, we were led to reexamine the reaction between atomic Ti and N_2O. Several studies concerning this system or the complementary one TiO + N_2 trapped in Ar [1] or Ne [2] matrices have been recently published.

The gas phase reactivity between transition metal (TM) atoms and nitrogen oxides was first considered at the end of the eighties[3] and widely developed in the nineties. In 2003, Campbell listed 29 TM (including some lanthanides) whose reactivity with respect to N_2O has been examined.[4] Despite the exothermicity of the dissociation reaction with formation of N_2 and TM monoxide, it was concluded that most of the TM atoms in their ground state (GS) are unreactive due to the existence of an activation barrier estimated between some units and some tens of kJ/mol (with the exception of V, Nb and La for which this barrier is close to zero).

Honma[5] has studied the reactivity of titanium atoms in ground (a^3F) and excited (a^5F) states with different ligands such as NO, CO_2, and N_2O. In line with previous works,[3,6] he showed that the excited state reacts much efficiently with all OX to give either the direct abstraction of an O atom, or the charge transfer to form $Ti^+ + OX^-$ followed by transfer of O^- to Ti^+. Therefore, the inefficiency of Ti(a^3F) with respect to Ti(a^5F) could be explained by the attractive character of this latter (Ti(a^5F, $3d^34s^1$)) and the repulsive one of the ground state (Ti(a^3F, $3d^24s^2$)). These conclusions have been confirmed by theoretical works of Pierloot,[7] who concluded that the $3d^{n+1}4s^1$ configuration gives rise to a higher reactivity than the $3d^n4s^2$ configuration.

Another experimental approach to the problem of the TM−N_2O reactivity has been used on the basis of the matrix isolation technique. The results vary according to the TMs: either weak interaction, of van der Waals type, for Ni, Pd, Pt[8] and Rh, Ru[9] with linear structures TM-NNO, or ionic pair for Au,[10] or direct insertion O−TM−N_2 for Mo, W[11] and for Ti.[1] It appears that the last conclusion on the direct Ti insertion in the N_2O, without any activation barrier, is at variance with the gas phase data[5] and throws some doubt on the validity of this matrix technique for studying reactions with low energy transition states. Although our main goal is to show that the origin of the discrepancy comes from the laser ablation technique for the sublimation of the metal atoms, which provides enough energy to promote the metal atoms in their excited states,[12] we also evidence the reliability of the double-hybrid functional to provide accurate descriptions of the electronic structure provided that we use an enough large basis set. The paper is organized as follows. After a short description of the experimental technique, the experimental results concerning the reactions between atomic Ti and one N_2O molecule, then between OTi and N_2, will be reported. They

Received: September 27, 2012
Revised: January 8, 2013
Published: January 25, 2013

include the description of selective irradiations which lead to the identification of three different one to one species. In a final part, theoretical calculations concerning geometrical, energetic and vibrational properties are developed and compared to the experimental data.

EXPERIMENTAL AND COMPUTATIONAL DETAILS

Experimental Details. The samples were prepared by co-condensing Ti vapor and dilute N_2O−Ne mixtures (100−2000 ppm N_2O in Ne) or, in some experiments, TiO vapor and dilute N_2−Ne mixtures (500−2000 ppm N_2 in Ne) onto one of six flat, highly polished, Rh-plated copper mirrors maintained at 3 K using a closed-cycle cryogenerator (model PT405, Cryomech, Syracuse, NY, USA). The sublimation of the solids was carried out in a liquid nitrogen-cooled trap minimizing outgassing impurities. A Ti−Mo filament (Goodfellow, 85% Ti) or effusion cell containing TiO powder (Alfa Aesar 99.5%) was heated at about 1500 °C to generate Ti or TiO vapor, respectively. Dismutation of TiO into Ti + TiO_2 was found negligible. The Ti or TiO deposition rate was monitored by a quartz microbalance and varied between 100 and 600 nmol/h. Three varieties of nitrous oxide, $^{14}N_2O$ (Alfa Gaz, 99.998%), $^{15}N_2O$ (Campro Scientific Gmbh 98%), and $^{14}N^{15}NO$ (Cambridge Isotope Laboratories 98%), and two varieties of dinitrogen, $^{14}N_2$ (L'Air Liquide, 99.998%) and $^{15}N_2$ (Isotec, 99.0%), were used as purchased. They were diluted in high purity neon (L'Air Liquide, 99.9995%) in a vacuum line connected to the cryogenerator through a high accuracy flowmeter. The gas flow rate was set to 5 mmol/h.

In general, after 90 min of deposition, infrared spectra of the resulting samples were recorded at 3 K, in the transmission−reflection mode between 9000 and 50 cm^{-1} using a Bruker 120 FTIR spectrometer and suitable combinations of Ge/KBr or Si/Mylar composite beamsplitters with either liquid N_2-cooled InSb or narrow band liquid N_2-cooled HgCdTe photoconductor or a liquid He-cooled Si−B bolometer with a 4 K-cooled 660 cm^{-1} low pass filter. In any case a globar was used as the source, which minimizes the risk of photolysis during spectral recording. The resolution was varied between 0.01 and 0.1 cm^{-1} in the near and mid-infrared and set to 0.5 cm^{-1} below 550 cm^{-1}. The frequency accuracy is ±0.1 cm^{-1} for narrow lines (±0.01 cm^{-1} for the TiO stretching multiplet recorded at 0.01 cm^{-1} resolution) and ±0.2 cm^{-1} for broader bands. The band area accuracy is on the order of 20% in the best cases but not better than 100% in the case of poor signal-to-noise ratio, corresponding to very weak absorbances. Also, note that the absorption spectra in the mid- and far-infrared were collected on the same samples through either CsI or polyethylene windows mounted on a rotatable flange separating the interferometer vacuum (5×10^{-3} mbar) from that of the cryostatic cell (10^{-7} mbar). The samples were subjected to irradiation from the near-infrared to the near-ultraviolet using broad or narrow band-pass filters and a W-wire or a 200 W Hg−Xe high-pressure arc lamp as light sources. The most significant results only will be described below.

Computational Details. All calculations have been performed using some hybrid (B3LYP and mPW1LYP) and a couple of double hybrid (mPW2PLYP,[13] B2PLYP,[14] and with their dispersion corrected variant: mPW2PLYP-D and B2PLYP-D[15]) functionals as well as the second order Møller−Plesset perturbation theory as implemented in the Gaussian 09 package.[16] The double-hybrid functionals include a second-order perturbation correction for nonlocal correlation effects and also a large contribution of the exact exchange (∼60%).[14]

The extended basis of Dunning's correlation-consistent polarized valence triple-ζ basis set (Aug-cc-pVTZ[17]) was used. In some cases, we used also the Ahlrichs basis set (TZVP[18]) and the Pople's ones (6-311+G(d) and 6-311+G-(2d)[19,20]). These basis sets are hereafter referred to as AVTZ, TZVP, Pop(d) and Pop(2d), respectively.

Stationary points were confirmed to be either minima (no imaginary frequency) or first-order saddle points (one imaginary frequency) by calculation of their vibration frequencies within the harmonic.

Furthermore, the monoreference character of the singlet state of the studied isomers has been investigated using the HOMO−LUMO mixing technique with density functional and also using the CASSCF (Complete Active Space SCF) approach with the Gaussian 09 package. As expected, a singlet state is considered as an open-shell singlet state when the expected value of spin square calculated with a monoreference method is not strictly equal to zero within the broken-symmetry framework. An MC-SCF (MultiConfiguration SCF) calculation provides a sure and definitive description of the mono- or multireference character of an electronic state. In our work, the active space is formed with four electrons in combination with ten orbitals, CASSCF(4,10).

EXPERIMENTAL RESULTS

One will describe successively the results obtained for the Ti/N_2O and TiO/N_2 doped Ne matrices, the first system having been studied more extensively than the second one, in particular at very low concentration in dopants to facilitate the identification of the spectra of the low-stoichiometry species.

1. Ti/N_2O/Ne System. *1.1. Concentration and Annealing Effects.* Ti vapor was condensed with relatively dilute mixtures of N_2O in Ne at 3 K. Several absorptions were detected (Table 1 and Figure 1-a) in the NN stretching region: a broad one at about 2248 cm^{-1} (Figure 1A), a sharper one at 2221 cm^{-1}

Table 1. Observed Absorptions (cm^{-1}) for vdW, End-on and Side-on Trapped in Ne at 3 K

assignment	vdW	^{3}[OTi(η^1-NN)])	^{1}[OTi(η^2-NN)])
ν_{TiN}		177.4[b]	
		185.4[b]	
δ_{NNO}	582.7		
ν_{TiO}		978.35[a]	980.1
$2\delta_{NNO}$	1158.9		
ν_{NNO} sym	1277.0		
$2\nu_{TiO}$		1950.7	1952.0
ν_{NN}	2221.0[a]	2246.9[b]	1699.4
		2249.8[b]	
$\nu_{NN} + \nu_{TiN}$		2429.7[b]	
		2432.7[b]	
$2\nu_{NO}$	2547.7		
$\nu_{NN} + \delta_{NNO}$	2789.4		
$\nu_{NO} + \nu_{NN}$	3474.3		
$2\nu_{NN}$	4412.0	4425.6[b]	3383.6
		4433.2[b]	

[a]Main component of a multiplet. Frequency accuracy improved by recording the spectrum at 0.01 cm^{-1} resolution. [b]Two values reported for these modes are due to site effects.

dx.doi.org/10.1021/jp309601e | J. Phys. Chem. A 2013, 117, 1697−1705

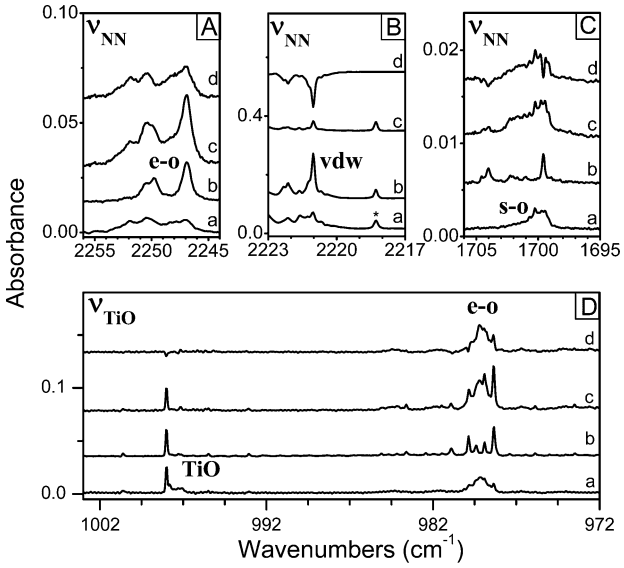

Figure 1. Development of the ν_{TiO} band of e-o and ν_{NN} band of vdW, e-o and s-o after deposition at 3 K (a), after annealing at 10 K (b), and after 64 min irradiation (c) (A, B, and D at 514 nm, C between 1.3 and 1.8 μm). (d) Difference between (c) and (b). The ν_3 band of unreacted $N_2{}^{18}O$ is labeled by an asterisk. Ti/N_2O/Ne = 0.2/0.5/1000.

(Figure 1B), and a weak broad one at about 1699 cm^{-1} (Figure 1C). As we will discuss later, these bands correspond respectively to three species: an [OTi(η^1-NN)] end-on (labeled as e-o), a van der Waals complex (vdW), and an [OTi(η^2-NN)] side-on (s-o). After deposition, the integrated intensity ratio of these bands stands around of 1/0.7/0.1, whatever the concentration in dopants. Consequently, we emphasize that the third band (1699 cm^{-1}) is substantially weaker than the first one (2248 cm^{-1}). In the TiO stretching region, we observed also after deposition the TiO diatomics fundamental at 998 cm^{-1}, and a broad band at 978 cm^{-1} 3 times stronger (Figure 1D). For the TiO stretching band, a possible Ti isotopic structure is expected. We observed a main triplet at 979.88, 979.40, and 978.35 cm^{-1} accompanied by four satellite triplets with the same structure. More precisely, the intensities of the five correlated components at 985.61, 982.44, 979.88, 977.40, and 975.03 cm^{-1} are found in the intensity ratio 0.115/0.105/1/0.074/0.074, close to the isotopic abundance ratio of natural Ti: 0.112/0.101/1/0.073/0.070 for $^{46}Ti/^{47}Ti/^{48}Ti/^{49}Ti/^{50}Ti$.

After studying the concentration dependence of these bands over a wide range, it appears that these four bands have the same linear dependence with respect to N_2O or Ti concentration. In line with a recent work of Zhou,[2] we can assign the bands at about 2248 cm^{-1} and 978 cm^{-1} to the NN and TiO stretchings of the [OTi(η^1-NN)] species,[2] hereafter referred to as end-on (e-o) compound and the band around 1699 cm^{-1} assigned to the NN stretching of the [OTi(η^2-NN)] species,[1] hereafter referred to as side-on (s-o) compound.

Concerning the fourth band (2221 cm^{-1}), observed for the first time in this work, we note a strong growth upon annealing at 10 K with a structure of multiplet that spreads over some cm^{-1} and displays a main component at 2221.0 cm^{-1} with a full width at half-maximum (FWHM) of 0.10 cm^{-1} (Figure 1B-b). In the same annealing conditions, the well-defined absorption around 2248 cm^{-1} slightly grows up, but not at the same rate as the 2221 cm^{-1} signal, and is structured in a main doublet at 2249.8−2246.9 cm^{-1}, 0.9 cm^{-1} FWHM for each component (Figure 1A-b). Upon annealing at 10 K, a multicomponent signal in the range 982−978 cm^{-1} (Figure 1D-b) also grows up at the same rate as the main doublet observed at 2249.8−2246.9 cm^{-1}. It is constituted of a main triplet at 979.88, 979.40, and 978.35 cm^{-1} (0.09 cm^{-1} FWHM for each component) accompanied by four satellite triplets with the same structure, two with frequency higher and two with frequency lower than the main triplet.

In the same annealing conditions, the broad band around 1699 cm^{-1} becomes essentially a narrow band and a doublet close to 1704 cm^{-1} appears (Figure 1C-b). This doublet does not correlate with end-on neither with side-on species. Because it appears only upon annealing, it is presumably due to $(Ti_x(N_2O)_y)$ aggregate with $x \geq 2$ and $y \geq 2$.

Also, much weaker absorptions in both the far- and near-infrared ranges (Figure 2 and Table 1) can be correlated with the NN and TiO stretchings of the e-o species.

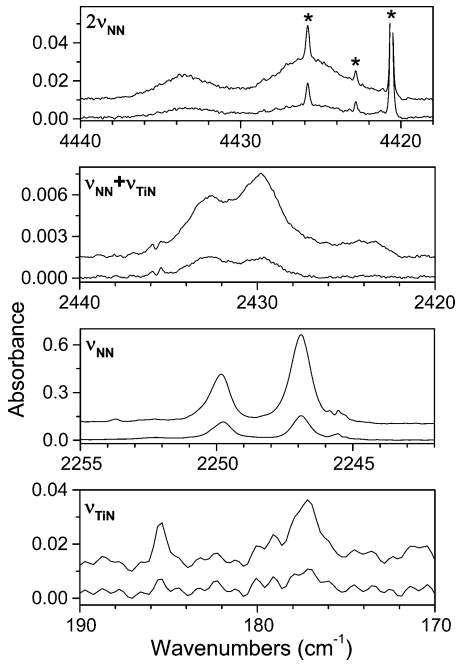

Figure 2. Typical absorption bands of e-o in various infrared regions for a Ti/N_2O/Ne = 0.2/0.5/1000 sample deposited at 3 K for 90 min. Displayed spectra are recorded at 3 K (a) after annealing at 11 K and (b) after irradiation in the visible. The $2\nu_{NN}$ bands of unreacted N_2O are labeled as asterisk.

More exactly, in the far-infrared only one transition, characterized by the doublet 185.4−177.4 cm^{-1}, has been identified. It correlates another doublet at 2432.7−2429.7 cm^{-1}, consistent with the combination of the ν_{NN} mode and the far-infrared doublet. In the near-infrared it is worth noting that the first overtone of ν_{NN} at 4433.2−4425.6 cm^{-1} is remarkable by its strong intensity (one-fifth of the fundamental) and by its position from which a large value of the anharmonicity coefficient is deduced (−33 cm^{-1} instead of −14.46 cm^{-1} observed for the free N_2 molecule).

1.2. Isotopic Effects. The experiments were repeated using isotopically labeled N_2O: $^{15}N_2O$ and $^{14}N^{15}NO$. The results are presented in Table 2. The NN stretching band of e-o and vdW for $^{15}N_2O$ is in a frequency ratio close to the square root of the inverse of their reduced mass ($(14/15)^{1/2}$ = 0.966), consistent

dx.doi.org/10.1021/jp309601e | J. Phys. Chem. A 2013, 117, 1697−1705

Table 2. Experimental Frequencies and Theoretical Harmonic Vibrational Data (cm^{-1}) of Studied Species, with the Isotopic Shifts (Relative Intensities in Parentheses)

		experiment			B2PLYP/AVTZ		
	mode	$^{14}N^{14}NO$	$^{14}N^{15}NO^{e}$	$^{15}N^{15}NO^{e}$	$^{14}N^{14}NO$	$^{14}N^{15}NO^{e}$	$^{15}N^{15}NO^{e}$
^{1}[OTi(η^2-NN)])	ν_{TiO} str	980.1 (22)	0	−0.2	979 (53)	0	0
	ν_{NN} str	1699.4 (100)[a]	−27.8	−56.4	1677 (100)	−28	−56
^{3}[OTi(η^1-NN)])	ν_{TiN} str	177.4 (12)	−1.6	−3.1	179 (9)	−2	−4
	ν_{TiO} str	978.3 (47)	0	0	996 (96)	0	0
	ν_{NN} str	2246.9 (100)[a]	−36.0[b]	−74.2	2282 (100)	−38[b]	−77
			−37.5[c]			−39[c]	
vdW	δ_{NNO} bend.	582.7 (1)	−13.3	−16.7	596 (1)	−13	−19
	ν_{NNO} sym str	1277.0 (22)	−4.7	−19.3	1297 (13)	−1	−19
	ν_{NN} str	2221.0 (100)[a]	−45.9	−69.0	2257 (100)	−49	−71
N_2O	δ_{NNO} bend.	591.2			599		
	ν_{NNO} sym str	1285.5			1298		
	ν_{NN} str	2225.3			2259		
N_2		2330[d]			2341		
TiO		1000[d]			1017		

[a]Relative IR intensities (with respect to the strongest fundamental of each specie: ν_{NN} ($I\nu_{NN}$ = 100)). [b]Isotopic shift for e-o OTi^{14}N^{15}N. [c]Isotopic shift for e-o OTi^{15}N^{14}N. [d]Taken from ref 23. [e]The isotopic shift using $^{14}N^{15}NO$ or $^{15}N_2O$ with respect to $^{14}N_2O$.

with a NN stretching mode. Also, with the $^{14}N^{15}NO$ isotope, we observed for e-o a small splitting of 1.5 cm^{-1} due to the existence of two nonequivalent molecules: $^{14}N^{15}NTiO$ and $^{15}N^{14}NTiO$. No splitting is observed for s-o. Also, the isotopic shifts for the 2221 cm^{-1} band are very similar, within experimental errors, in comparison with the isotopic shifts for the ν_3 band of unreacted N_2O. Accordingly, we conclude that the band at 2221.0 cm^{-1} corresponds to the NN vibration of a very weakly perturbed N_2O moiety, thus attributable to a molecular complex of van der Waals type with one titanium atom and one N_2O molecule, not observed previously.

1.3. Photochemical Conversions between the Different Forms of the Ti/N_2O Pair. The improvement in the assignment of the spectra of the two species identified so far is based on the photoconversion vdW → e-o upon selective irradiation in the visible and near-ultraviolet. This conversion allows identification of eight transitions of vdW and six of e-o. On the other hand, a totally different conversion is observed when the sample is submitted to irradiation in the range 1.3−1.8 μm. Indeed, vdW remains unchanged whereas e-o is converted into s-o. Also, a band at 980.1 cm^{-1} behaved similarly upon this selective irradiation to the band of the s-o at 1699.4 cm^{-1}.

1.3.1. vdW → e-o Conversion. The Figure 1 shows an example of the vdW → e-o conversion for a long time irradiation. Parts A and B of Figure 3 display the effects of irradiation at 514 and 405 nm on the intensity of the N−N stretching bands (cm^{-1}) of the three species under scrutiny. The changes in band areas $\Delta S(t) = S(t) - S(0)$ versus the irradiation duration time t show a strong correlation between the positive values $\Delta S(t)$ of e-o and the negative value of vdW whatever t, the band area for s-o remaining roughly unchanged all along the irradiation process. Parts A and B of Figure 3 illustrate the case of irradiations at 514 and 405 nm during which the ν_{NN} multiplet characterizing vdW around 2221 cm^{-1} progressively disappears with concomitant increase of the one around 2248 cm^{-1} assigned to ν_{NN} e-o. Irradiation at 365 nm carried out at very low N_2O concentration (Figure 3C) shows significant differences with respect to those in the visible. On the one hand, the conversion is much faster, with a characteristic time of about 8 s against 15 min for 405 and 514 nm, respectively. On the other hand, when vdW has totally

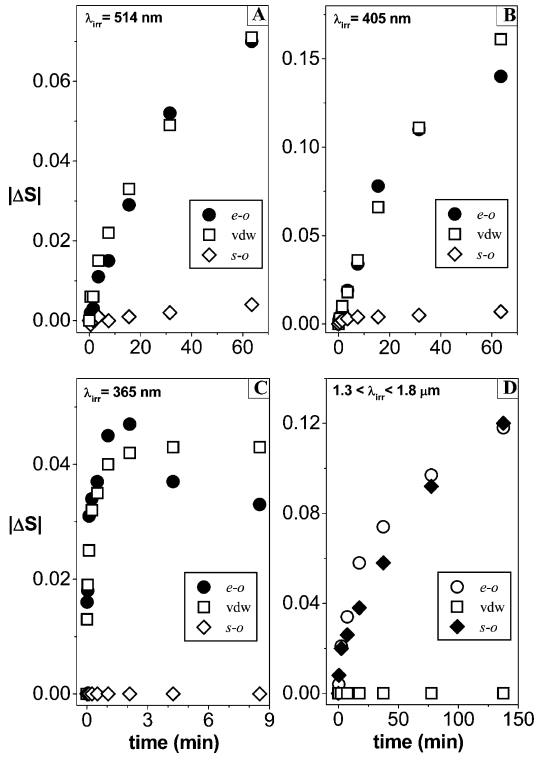

Figure 3. Time development of the irradiation-induced interconversions between the three forms of the Ti−N_2O pair trapped in Ne and carried out at 3 K. Ti/N_2O/Ne = 0.2/0.5/1000 (A), 0.2/1/1000 (B), 0.2/0.1/1000 (C), and 0.2/0.5/1000 (D). Samples deposited at 3 K and annealed at 11 K before irradiation. The changes in band areas $\Delta S(t) = S(0) - S(t)$ are negative for open symbols (◇, ○, □) and positive for solid symbols (◆, ●, ■).

disappeared (after about 100 s irradiation) the concentration of e-o starts decreasing without increase of s-o. One thus concludes that e-o is photolyzed by UV light, which is confirmed by the intensity increase of the band of free TiO at about 998 cm^{-1}:

$$[OTi(\eta^1 - NN)] \xrightarrow{UV} N_2 + TiO \quad (1)$$

dx.doi.org/10.1021/jp309601e | J. Phys. Chem. A 2013, 117, 1697−1705

Nevertheless, no change was observed upon 514 nm photolysis of the TiO band.

1.3.2. e-o → s-o Conversion. Some spectral effects in the domain 5500−7500 cm^{-1} (1.3−1.8 μm) for a long time irradiations are illustrated in Figures 1C and 4.

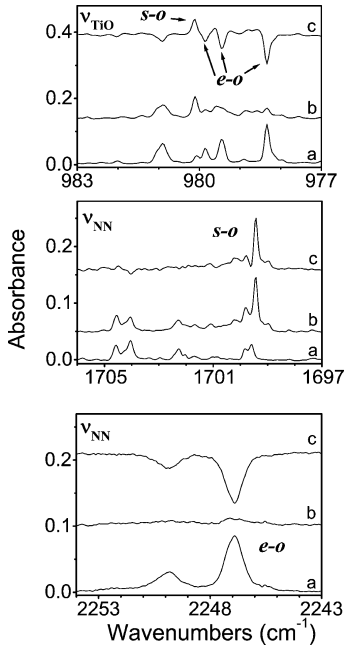

Figure 4. Development of the ν_{TiO} and ν_{NN} bands of s-o and e-o before (a) and after (b) 138 min irradiation between 1.3 and 1.8 μm, with the difference (c) = (b) − (a). Sample with $Ti/N_2O/Ne$ = 0.2/0.5/1000 deposited at 3 K for 90 min, recorded at 3 K after annealing at 11 K before irradiation.

Figure 1C displays only the growth up of NN band in s-o compound, whereas the spectral changes of the e-o and s-o species are shown in Figure 4 in the NN and TiO stretching regions.

Figure 3D displays the time dependence of the band areas upon exposure of the sample to irradiation. The reaction kinetic reported in Figure 3D clearly evidence that the concentration of vdW remains perfectly unchanged upon irradiation, whereas those of e-o and s-o vary as $2\Delta S(t)_{s\text{-}o} = -\Delta S(t)_{e\text{-}o}$.

1.3.3. Irradiations in the Intermediate Range 1000−700 nm. During the deposition process which lasts about 1 h the sample is submitted to the irradiation from the Ti/Mo filament heated to ∼1800 K, which emits significantly in the very near-infrared. To confirm the effect of this indirect irradiation, we decided to irradiate our sample using a pass band filters transmitting between 700 and 1000 nm. Our observations could be summarized in two points:

1. The vdW bands decrease in intensity while those of e-o and s-o increase, but at a rate 1 order of magnitude smaller than that of vdW.
2. The diatomic TiO band increases slightly with this irradiation.

Due to this experience, one can easily conclude that the vdW complex is actually sensitive to the irradiations in the very near-infrared range. We can thus explain why the e-o and s-o complexes and the TiO diatomic are detected just after deposition. Indeed, a non-negligible part of the vdW complex can be converted predominantly into e-o complex and diatomic TiO, and slightly into s-o complex. The vdW photoconversion occurs in two steps:

- First, the N−O bond of vdW complex is cleaved under 1000−700 nm irradiations leading to the formation of two diatomic species: TiO and N_2.
- Second, a large part of TiO reacts with N_2 molecules to yield predominantly e-o and slightly s-o complexes.

As an additional point, the observation of the TiO band after deposition indicates that the second step is not fully efficient.

2. $TiO/N_2/Ne$ System. The spectra observed after deposition and their evolution upon annealing are close to those reported by Zhou,[2] who have identified e-o by its NN and TiO stretching modes at around 2250 and 980 cm^{-1}. In the NN stretching region of free N_2, around 2330 cm^{-1}, we were unable to detect any signal typical of a metastable unreacted $TiO\text{-}N_2$ pair. Because the e-o bands grow upon annealing, we thus conclude that the formation of e-o does not require activation energy. Here again the observation of photoconversion processes allows us to improve the assignment of the spectrum of e-o and to identify some bands of s-o not present after annealing.

In the case of irradiation at 365 nm, the absence of vdW as reservoir for the formation of the e-o species leads to the intensity decrease of the bands assigned to e-o from the beginning of the experiment, with concomitant increase of the free TiO band around 998 cm^{-1}. This result confirms our observation described in 1.3.1 (eq 1). For irradiations in the near-infrared, the e-o → s-o photoconversion is clearly evidenced. Figure 5 displays the conversion observed after 7.5 min in the range 5500−10000 cm^{-1} (1.1−1.8 μm). We can clearly note that the e-o doublet detected in the NN stretching region (2249−2246 cm^{-1}) decreases upon irradiation by a factor of 3 whereas the corresponding mode of s-o (1702−1699 cm^{-1}), negligible just after deposition, significantly increases after irradiation.

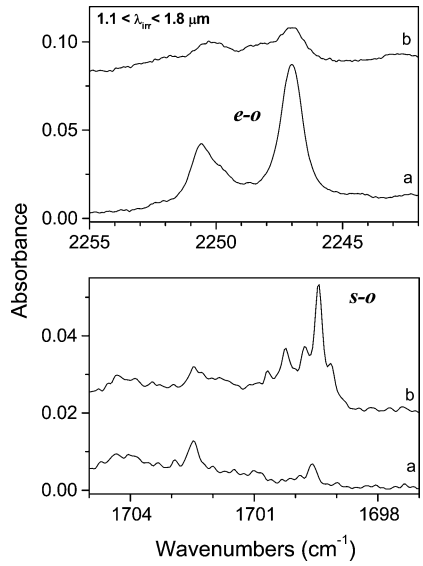

Figure 5. Variation of the ν_{NN} band of s-o and e-o from the reaction TiO + N_2 in solid neon (lower and upper frame, respectively), after irradiation in the near. Sample with $TiO/N_2/Ne$ = 0.25/1/1000 deposited at 3 K for 90 min (a) and after irradiation (b).

dx.doi.org/10.1021/jp309601e | J. Phys. Chem. A 2013, 117, 1697−1705

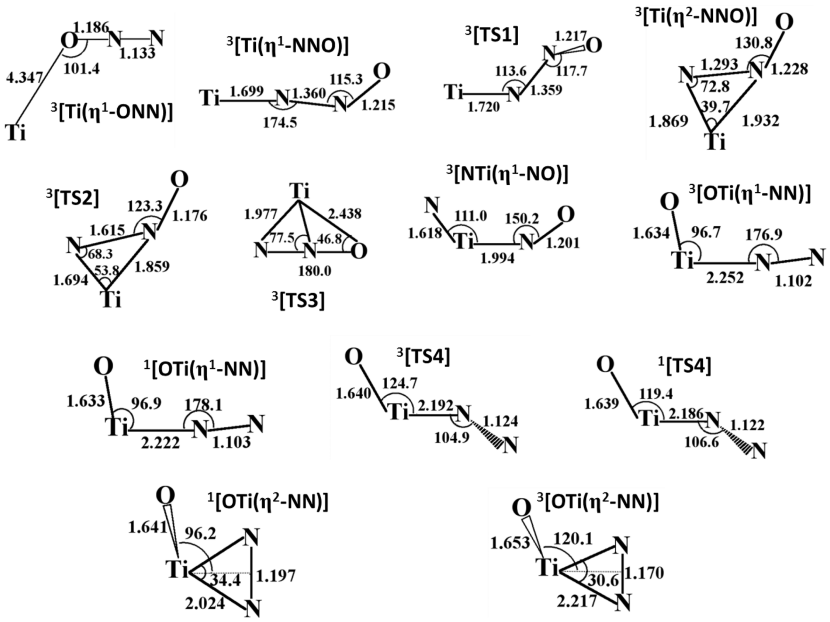

Figure 6. Structural parameters of all the stationary points obtained at the B2PLYP/AVTZ level. Distances are given in Å and angles in degrees.

THEORETICAL RESULTS

Several coordination approaches on the Ti/N_2O and TiO/N_2 binary reagents have been investigated. Figure 6 displays all thirteen fully optimized geometries at the B2PLYP/AVTZ level of theory. Five of the thirteen stationary points have one imaginary frequency (transition state) and eight others correspond to the local or global minima on the potential hypersurface. Over the eight latter structures, three correspond to the Ti/N_2O adduct complexes optimized only in the triplet spin state which are labeled as follows: ^{3}[Ti(η^1-ONN)], ^{3}[Ti(η^1-NNO)], and ^{3}[Ti(η^2-NNO)]. The other five minima correspond to the insertion products involving TiO/N_2 subunits in both triplet and singlet states (^{1,3}[OTi(η^1-NN)] and ^{1,3}[OTi(η^2-NN)]) and NTi/NO subunits in only triplet state (^{3}[NTi(η^1-NO)]).

One of the five optimized transition states (^{3}[TS1]) connects the two adduct complexes together, ^{3}[Ti(η^1-NNO)] and ^{3}[Ti(η^2-NNO)]. Transition from the ^{3}[Ti(η^2-NNO)] minima toward an inserted product is explored using two transition states (^{3}[TS2] and ^{3}[TS3]) leading to the ^{3}[NTi(η^1-NO)] and ^{3}[OTi(η^1-NN)], respectively. Finally, the isomerization process between two inserted products involving TiO/N_2 subunits has been fully characterized by two transition states, (^{3}[TS4] and (^{1}[TS4]), on the triplet and singlet states, respectively. In the following, we restrict our study only to the experimentally observed species in the neon matrix, labeled as e-o, s-o, and vdW. These products correspond to three of the optimized geometries: two inserted products, ^{3}[OTi(η^1-NN)] and ^{1}[OTi-(η^2-NN)] and one van der Waals complex^3[Ti(η^1-ONN)].

1. Geometrical Structures. Most relevant geometrical parameters calculated with the double-hybrid functionals are gathered in Figure 7. These data have been obtained using the AVTZ basis set and B2PLYP, B2PLYPD, mPW2PLYP, and mPW2PLYPD, respectively, from top to bottom.

1.1. ^{3}[OTi(η^1-NN)]. The triplet e-o compound is found to be in the C_s symmetry with a planar geometry. The $\angle$ $\overline{\text{OTiN}}$ angle is almost 96° for all the used functionals. The Ti−N and N−N bond lengths are very insensitive to the dispersion corrected of

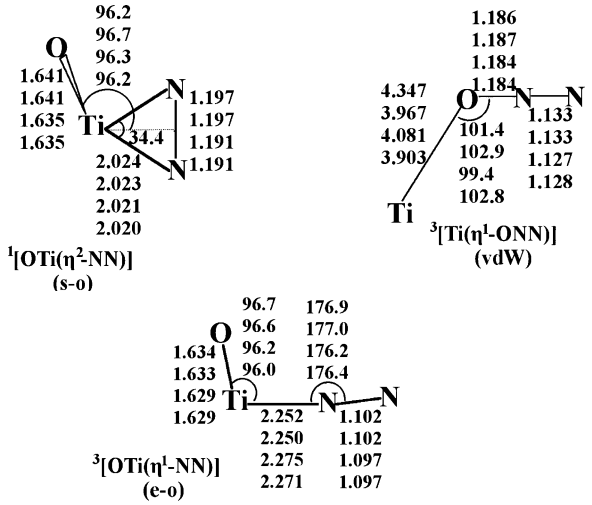

Figure 7. Optimized parameters of the three observed species (s-o, e-o inserted compounds, and vdW complex) calculated with double hybrid functionals. Reported values, from top to bottom, are obtained with B2PLYP, B2PLYPD, mPW2PLYP and mPW2PLYPD functionals, respectively using the AVTZ basis set. Distances are in Å and angles in degrees.

both B2PLYP and mPW2PLYP. Nevertheless, the Ti−N distance optimized with B2PLYP is actually shorter than that obtained with mPW2PLYP. Consequently, we found a slightly longer N−N bond length with B2PLYP than with mPW2PLYP.

1.2. ^{1}[OTi(η^2-NN)]. The singlet s-o structure has an out of plane geometry in the C_s group. Its $\angle$ $\overline{\text{OTiNN}}$ dihedral angle is about 96°. There is no effect of the dispersion correction on the geometrical parameters, similar to the e-o structure. The Ti−N bond length optimized with B2PLYP is now very slightly longer than that obtained with mPW2PLYP. We note a very small change in the N−N distance when both functionals are used.

1.3. vdW Complex ^{3}[Ti(η^1-NNO)]. Unlike previous structures, here the Ti atom is bonded to the oxygen side of N_2O. This complex is characterized by a large Ti−O distance (∼4 Å) and a bent structure (/ $\overline{\text{TiON}}$ ∼100°), whereas the ONN

dx.doi.org/10.1021/jp309601e | J. Phys. Chem. A 2013, 117, 1697−1705

partner is left almost linear (∠ $\overline{ONN}$ ~179.6°). As expected, it should be highlighted that the Ti−O bond length is very sensitive to the dispersion correction in the functional (4.347 vs 3.967 Å for B2PLYP and B2PLYPD, and 4.081 vs 3.903 Å for mPW2PLYP and mPW2PLYPD), whereas the N−N distance is left unchanged (1.133 and 1.128 Å with B2PLYP and mPW2PLYP, respectively). The ∠ $\overline{TiON}$ angle was found to be 101, 103, 99 and 103° with B2PLYP, B2PLYPD, mPW2PLYP, and mPW2PLYPD, respectively. We note that the dispersion correction effect on this angle is almost negligible (2 and 4°).

Indeed, we can clearly conclude that the dispersion term does not improve the results and then its use is not necessary for the studied cases.

2. Energetic Analysis. In a previous theoretical work,[2] Zhou and co-workers performed some calculations on the ^{3}[OTi(η^1-NN)], ^{1}[OTi(η^2-NN)] structures using two hybrid functionals (B3LYP and mPW2PLYP) and the 6-311+G(d) basis set. They concluded that the triplet end-on structure (^{3}[OTi(η^1-NN)]) corresponds to the ground electronic state and is slightly more stable than the singlet side-on structure (^{1}[OTi(η^2-NN)]) by around 2.0 or 0.5 kcal/mol depending to the functional used. Because the double hybrid functionals due to the MP2 contribution are more basis set size dependent than the traditional hybrid ones, we performed also additional calculations using different basis sets. In Table 3 are reported

Table 3. Basis Set Size Effect on the Energetic Gap, ΔE (kcal/mol), of the Two Most Relevant Structures (ΔE = $E(^1$[OTi(η^2-NN)]) − $E(^3$[OTi(η^1-NN)]))

	TZVP	Pop(d)	Pop(2d)	AVTZ
	90/19[a]	124/202[a]	146/230[a]	231/605[a]
mPW2PLYP	+2.8	+0.5	+0.2	−0.3
B2PLYP	+0.8	−1.2	−1.8	−2.3
mPW1LYP	+4.8	+3.3	+3.0	+3.4
B3LYP	+3.1	+1.7	+1.4	+1.9
MP2	+2.3	−1.5	−2.8	−6.4

[a]Basis functions/primitive gaussians.

the relative energies (in kcal/mol) between the side-on and end-on structures, ΔE = $E(^1$[OTi(η^2-NN)]) − $E(^3$[OTi(η^1-NN)]), calculated with two hybrids, two double-hybrid functionals, and MP2 methods using different basis sets. We observe that the singlet side-on structure is less stable than the triplet end-on one whatever the hybrid functional and/or basis set. Contrarily, for the MP2 method the singlet side-on structure is now more stable than the triplet end-on one, with the exception of TZVP basis set which gives the same result than the hybrid functional. Consequently, it is quite normal that the double-hybrid functional results lie between hybrid functional and MP2 ones. The conclusion is therefore straightforward: a quantitatively well description of the studied compounds requires the use of large basis set with double-hybrid functionals. Particularly, we note that the B2PLYP functional is more suitable for this study than the mPW2PLYP one. The energetic gap is well converged and the calculated vibrational analysis is in good agreement with the experimental one (vide infra) when we use the B2PLYP functional.[21]

Due to a partially filled d subshell, the transition metal containing compounds often have several low-lying nearly degenerate states. For such systems, a quantitatively accurate description of the electronic structure requires the inclusion of both dynamical and static electron correlations. In contrast with the wave function based methods for which the inclusion of multiple configurations in a well balanced way remains a difficult task to achieve, the DFT approach offers a simple and surprisingly accurate alternative for such systems.[22] To determine the mono- or multireference nature of our systems, we used two techniques: the HOMO−LUMO mixing technique and the CASSCF method.

- In the first approach, we can mix the HOMO and LUMO using the singlet monodeterminantal wave function to check the stability of the SCF solution. This procedure is particularly useful when the energetic gap between two singly occupied molecular orbitals (SOMO) is less than 1 eV. Consequently, the HOMO−LUMO mixing leads to a spin contamination, $\langle S^2_{(Singlet)}\rangle \neq 0$, predicting a multireference character for the singlet state. Two singlet structures, end-on ^{1}[OTi(η^1-NN)] and side-on ^{1}[OTi(η^2-NN)], have been investigated with this approach. It has been shown that the closed-shell wave function of the side-on structure is stable with respect to any orbital mixing without spin contamination. For the end-on structure, the stability test results to an RHF-to-UHF instability. We found a stable unrestricted wave function characterized by a spin contamination, $\langle S^2_{(Singlet)}\rangle = 1.006$, indicating a strong biradical character. The importance of this latter could be estimated with the calculated natural orbital occupation numbers (NOON): 1.00 and 1.00 electrons in the 22th and 23th natural orbitals.
- Furthermore, calculations performed at the CASSCF-(4,10)/Pop(2d) level of theory at the B2PLYP/Pop(2d) optimized geometries provide the same description as the HOMO−LUMO mixing one. In the case of the side-on structure, we found that the SCF reference accounts for 86% of the CI wave function. It is interesting to note that the contribution of double excited configurations amounts to 13%. In such a case, the use of double hybrid DFT method allowed the dynamical correlation to be mostly recovered by the functional part and the static correlation due to the double excitations by the MP2 contribution. The calculated NOON values (1.92, 1.78, 0.22, and 0.08 electrons) testify that the biradical character of the singlet side-on structure is insignificant. Contrarily, the CAS calculations clearly evidence a multireference character of the singlet end-on structure. The CI wave function is composed of two main configurations (58% and 37%). The calculated NOON values (1.93, 1.20, 0.80, and 0.07) actually indicate the biradical nature of ^{1}[OTi(η^1-NN)], very close to the results of the DFT approach.

Consequently, we conclude that the double hybrid functional (B2PLYP) is adequate to treat our systems whatever the nature of systems: mono- (^{1}[OTi(η^2-NN)]) or multideterminant (^{1}[OTi(η^1-NN)]).

We turn now to the study of the reaction mechanisms for the formation of the two inserted species. In Figure 8 are reported the relative energetic values (in kcal/mol) with respect to free Ti + N_2O and to TiO + N_2, obtained at the B2PLYP/AVTZ level of theory. On the ground of the energetic results, we can summarize our discussion as follows:

dx.doi.org/10.1021/jp309601e | J. Phys. Chem. A 2013, 117, 1697−1705

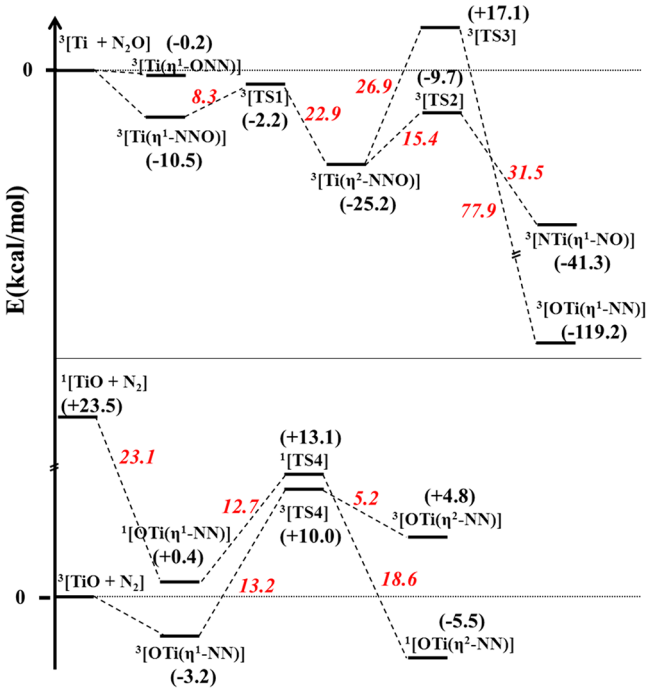

Figure 8. The energetic pathway for the Ti+N_2O and TiO+N_2 reactions. Relative energies are given in kcal/mol at the B2PLYP/AVTZ level.

- In the first pathway for the Ti/N_2O reaction, the reaction proceeds only in the triplet surface. Two final structures are present, the ^{3}[NTi(η^1-ON)] and ^{3}[OTi(η^1-NN)]. The latter was found to be much more stable (119 vs 41 kcal/mol), which confirm its experimental observation.
- Along the second pathway OTi ($^3\Delta$)/N_2 ($^1\Sigma_g^+$) reaction, we found two minima (e-o and s-o) for each spin multiplet with suitable transition state. The reaction actually starts on the triplet surface (in the entrance channel) to finish on the singlet state (final product): two-state reactivity. We note that the singlet s-o ground state is only slightly 2.3 kcal/mol lower in energy than the triplet e-o intermediate.
- The transition state from the triplet e-o to the triplet s-o structure was found to be at least around 4600 cm^{-1}. We believe that this barrier height should be considered as a lower bound compared to the experimental photochemical conversion data (between 5500 and 7500 cm^{-1}).

EXPERIMENT VS THEORY

Vibrational analysis has been performed only with the B2PLYP approach within the harmonic framework. All the calculated and experimental frequencies as well as the isotopic shifts are reported in Table 3.

As discussed above, five main experimentally observed frequencies, located at 2246.9, 1699.4, 980.1, 978.3, and 177.4 cm^{-1}, have been assigned to two species containing explicitly the TiO and N_2 partners: two for the side-on ^{1}[OTi(η^2-NN)]) structure and three for the end-on ^{3}[OTi(η^1-NN)]) structure. Two frequencies (980.1 and 1699.4 cm^{-1}) corresponding to the TiO and NN stretching in ^{1}[OTi(η^2-NN)]) structure are red-shifted by 18 and 630 cm^{-1}, compared to free TiO and N_2 molecules. The NN red-shift is well reproduced (630 vs 664 cm^{-1}) whereas the TiO red-shift is overestimated by calculation (18 vs 38 cm^{-1}). In contrast, the relative experimental intensities of the TiO/NN stretching bands (22%) are not very well reproduced by calculation (53%).

The three other experimental vibrational frequencies (2246.9, 978.3, and 177.4 cm^{-1} have been assigned to the NN, TiO, and TiN stretching modes for the e-o species. The NN and TiO stretching modes are experimentally red-shifted by 83 and 22 cm^{-1} with respect to free molecules. Theoretically, the NN and TiO stretching are calculated to be red-shifted by 59 and 21 cm^{-1}, respectively. We can see that the TiO red shift is now well reproduced whereas the NN red shift is actually underestimated. Concerning the TiO and NN relative infrared intensities, here again the calculated TiO value (96%) is nearly twice overestimated compared to the experimental one (47%).

For the vdW complex, the experimental vibrational properties are fairly well reproduced by B2PLYP functional. Compared to free N_2O, the experimental frequencies of vdW complex are red-shifted by about 8.5, 8.5, and 4.3 cm^{-1}, respectively for the NNO bending, NNO symmetric and asymmetric stretchings. Our calculations predict also small red shifts for these modes (3, 1, and 2 cm^{-1}).

Concerning the isotopic shifts with $^{14}N^{15}NO$ and $^{15}N_2O$, a very good agreement has been found between experimental and theoretical results.

CONCLUSIONS

In this paper we reported experimental and theoretical data on the reactivity of the titanium atom with N_2O. The most significant conclusions are as follows:

1. In the neon matrix, we observed the coexistence of a vdW complex (^{3}[Ti(η^1-ONN)]) and an end-on species (^{3}[OTi(η^1-NN)]) after thermal deposition of Ti and N_2O at 3 K. A third species, ^{1}[OTi(η^2-NN)] is also present in a very weak quantity.
2. The presence of the vdW complex just after deposition evidence the nonreactivity of Ti(a^3F) atoms with N_2O, as already proved in previous gas phase experiment. Furthermore, the formation of such a complex put into consideration the important role of the metal's deposition way.
3. To confirm our finding on the insertion complexes, we also studied the OTi + N_2 system in the neon matrix. We observed the coexistence of the end-on and side-on species, the last one in very weak quantities, and no trace of an OTi···N_2 vdW complex. It has been shown that the obtaining of an easily observable side-on species requires a photochemical conversion.
4. In line with the theoretical strategy of Zhou, we used the double hybrid functionals but with a large basis set. It has been shown that
   - the reaction between TiO and N_2 leads to end- and side-on complexes at both triplet and singlet electronic states,
   - the singlet s-o structure is the ground state when calculations are performed with a large basis set, whereas the triplet e-o complex is the low-lying intermediate.

dx.doi.org/10.1021/jp309601e | J. Phys. Chem. A 2013, 117, 1697−1705

- both HOMO−LUMO mixing and CASSCF(4,10) studies confirm the monoreference character of the singlet s-o,
- the isomerization e-o → s-o process requires an energy supply at least about 4600 cm^{-1}, in relatively good agreement with the experimental one (between 5500 and 7500 cm^{-1}),
- the N−N frequency gap between the e-o and s-o structures is calculated to be close to the experimental value (605 vs 548 cm^{-1}), and
- the double hybrid functionals are suitable to study appropriately the metal−ligand interactions, provided a large enough basis set is used. However, it has been observed that the B2PLYP functional reproduces the experimental values better than the mPW2PLYP one.

We are doing a systematic study with ab initio and DFT families to confirm these conclusions which will be published in a second paper.

■ ASSOCIATED CONTENT

Supporting Information

To help experimentalists for a future observation of ^{3}[NTi(η^1-NO)] and ^{3}[Ti(η^2-NNO)], the most relevant vibrational data are reported in Table S1 for two triplet intermediates formed in the entrance of reaction channel from the Ti + N_2O interaction. In Table S2 are gathered the vibrational data calculated with B3LYP/AVTZ and MP2/AVTZ for the two experimentally observed species. This material is available free of charge via the Internet at http://pubs.acs.org.

■ AUTHOR INFORMATION

Corresponding Author

*E-mail: M.E.A., esmail.alikhani@upmc.fr; B.T., benoit.tremblay@upmc.fr.

Notes

The authors declare no competing financial interest.

■ ACKNOWLEDGMENTS

The authors are grateful to Dr. Hélène BOLVIN (LCPQ of Toulouse) for helpful discussions and her technical helping on the CASSCF calculation.

■ REFERENCES

(1) Chen, M.; Wang, G.; Zhou, M. *Chem. Phys. Lett.* **2005**, *409*, 70.
(2) Zhou, M.; Zhuang, J.; Zhou, Z.; Li, Z. H.; Zhao, Y.; Zhen, X.; Fan, K. *J. Phys. Chem. A* **2011**, *115*, 6551.
(3) Ritter, D.; Weisshaar, J. C. *J. Phys. Chem.* **1989**, *93*, 1576.
(4) Campbell, M. L. *J. Phys. Chem. A* **2003**, *107*, 3048.
(5) Clemmer, D. E.; Honma, K.; Koyano, I. *J. Phys. Chem.* **1993**, *97*, 11480.
(6) Vetter, R.; Naulin, C.; Costes, M. *Phys. Chem. Chem. Phys.* **2000**, *2*, 643.
(7) Delabie, A.; Vinckier, C.; Flock, M.; Pierloot, K. *J. Phys. Chem. A* **2001**, *105*, 5479.
(8) Jin, X.; Wang, G.; Zhou, M. *J. Phys. Chem. A* **2006**, *110*, 8017.
(9) Jiang, L.; Xu, Q. *J. Phys. Chem. A* **2009**, *113*, 5620.
(10) Jiang, L.; Kohyama, M.; Haruta, M.; Xu, Q. *J. Phys. Chem. A* **2008**, *112*, 13495.
(11) Jiang, L.; Xu, Q. *J. Phys. Chem. A* **2010**, *132*, 164305.
(12) Kang, H.; Beauchamp, J. L. *J. Phys. Chem.* **1985**, *89*, 3364.
(13) Schwabe, T.; Grimme, S. *Phys. Chem.* **2006**, *8*, 4398.
(14) Grimme, S. *J. Chem. Phys.* **2006**, *124*, 034108.
(15) Schwabe, T.; Grimme, S. *Phys. Chem. Chem. Phys.* **2007**, *9*, 3397.
(16) Frisch, M. J.; Trucks, G. W.; Schlegel, H. B.; Scuseria, G. E.; Robb, M. A.; Cheeseman, J. R.; Scalmani, G.; Barone, V.; Mennucci, B.; Petersson, G. A.; Nakatsuji, H.; Caricato, M.; Li, X.; Hratchian, H. P.; Izmaylov, A. F.; Bloino, J.; Zheng, G.; Sonnenberg, J. L.; Hada, M.; Ehara, M.; Toyota, K.; Fukuda, R.; Hasegawa, J.; Ishida, M.; Nakajima, T.; Honda, Y.; Kitao, O.; Nakai, H.; Vreven, T.; Montgomery, J. A.; , Jr., Peralta, J. E.; Ogliaro, F.; Bearpark, M.; Heyd, J. J.; Brothers, E.; Kudin, K. N.; Staroverov, V. N.; Kobayashi, R.; Normand, J.; Raghavachari, K.; Rendell, A.; Burant, J. C.; Iyengar, S. S.; Tomasi, J.; Cossi, M.; Rega, N.; Millam, J. M.; Klene, M.; Knox, J. E.; Cross, J. B.; Bakken, V.; Adamo, C.; Jaramillo, J.; Gomperts, R.; Stratmann, R. E.; Yazyev, O.; Austin, A. J.; Cammi, R.; Pomelli, C.; Ochterski, J. W.; Martin, R. L.; Morokuma, K.; Zakrzewski, V. G.; Voth, G. A.; Salvador, P.; Dannenberg, J. J.; Dapprich, S.; Daniels, A. D.; Farkas, O.; Foresman, J. B.; Ortiz, J. V.; Cioslowski, J.; Fox, D. J.; *Gaussian 09*, Revision A.02; Gaussian, Inc., Wallingford, CT, 2009.
(17) Dunning, T. H., Jr. *J. Chem. Phys.* **1989**, *90*, 1007.
(18) Schaefer, A.; Huber, C.; Ahlrichs, R. *J. Chem. Phys.* **1994**, *100*, 5829.
(19) McLean, A. D.; G.S. Chandler, G. S. *J. Chem. Phys.* **1980**, *72*, 5639.
(20) Curtiss, L. A.; McGrath, M. P.; Blandeau, J.-P.; Davis, N. E.; Binning, R. C.; Radom, L., Jr. *J. Chem. Phys.* **1995**, *103*, 6104.
(21) Further arguments will be provided in a future publication devoted only to a systematic theoretical study with ab initio and DFT families to testify the choice of the B2PLYP functional.
(22) Cramer, C. J.; Truhlar, D. G. *Phys. Chem. Chem. Phys.* **2009**, *11*, 10757.
(23) Huber, K. P.; Herzberg, G. *Molecular Spectra and Molecular Structure Constant of Diatomic Molecules*; (van Nostrand Reinhold: New York, 1979.